Chapter 8
Expanding the Versatility of Resonant Ultrasound Spectroscopy

Andres Garcia, Kayleigh Hanlon, Matthew Luci, Mentors: Paul Geimer, Mathew Hayne, and Georgios Koutsakis

Abstract Resonant Ultrasound Spectroscopy (RUS) is used for the experimental characterization of materials. This method is traditionally performed in a free vibrating regime which requires that parts are removed from production which increases labor cost and analysis time. This project aims to expand RUS to accommodate non-ideal experimental boundary conditions. By integrating Finite Element Analysis (FEA) with RUS, we seek to explore the possibility of extracting accurate elastic property measurements of metallic samples that are clamped or otherwise constrained. Our experimental methods involve comparing the extracted material properties from freely vibrating metallic samples with those from constrained samples to determine the limitations of current RUS data extraction methods. While our team successfully extracted accurate material properties for freely vibrating samples, we encountered challenges with constrained samples due to RUS's limitations in handling transient terms and complex boundary conditions. Despite this setback, we gained valuable insights into the effects of boundary conditions, including damping produced at the contact interface and frequency shifts. Our results reveal the current limitations of RUS in scenarios involving constrained samples and highlight the need for further research and algorithm development. These advancements are necessary to overcome the existing constraints and enhance RUS's capabilities for more diverse experimental conditions.

Keywords Resonant ultrasound spectroscopy (RUS) · Acoustic excitation · Modal analysis · Finite element analysis (FEA) · Nondestructive testing · Boundary conditions

Introduction

RUS is a non-destructive testing method used to determine the mechanical properties of materials. It works by actively exciting a sample and measuring the natural resonance frequencies at which it vibrates. Researchers can then work backwards (via an "inversion" problem) to determine the material's elastic properties.

Figure 1 provides a detailed illustration of the typical RUS workflow [1]. Table 1 outlines fundamental RUS characteristics, while our research focused on modifications to boundary conditions, frequency spectra, and mode shapes. Traditional

Andres Garcia
Texas A&M University, College Station, TX 77843
e-mail: andresgar@lanl.gov

Kayleigh Hanlon
University of Illinois Urbana-Champaign, Urbana, IL 61801
e-mail: khanlon@lanl.gov

Matthew Luci
Rose-Hulman Institute of Technology, Terre Haute, IN 47803
e-mail: luci.m@lanl.gov

Paul Geimer · Mathew Hayne
Los Alamos National Laboratory, Los Alamos, NM 87545
e-mails: pgeimer@lanl.gov, mhayne@lanl.gov

Georgios Koutsakis
University of New Mexico, Albuquerque, NM 87131
e-mail: kousakis@unm.edu

Kristin B. Zimmerman, PhD (eds.), *Topics in Modal Analysis & Parameter Identification in Structural Dynamics, 2026, Vol. 8*,
Conference Proceedings of the Society for Experimental Mechanics Series, https://doi.org/10.1007/978-8-743-81447-4_8

RUS assumes the sample is freely vibrating and a simple geometry that is precisely shaped, but this limits what types of samples can be tested. To overcome this, researchers integrate FEA along with RUS. FEA helps simulate vibrations for samples with more complex shapes or boundary conditions, like partial constraints or supports. This combined method improves the flexibility of RUS and makes it more applicable to real-world situations. These real-world applications can range from identifying nonconformance in complex additive manufactured parts to determine the characteristics of an unknown material. However, while FEA has helped extend RUS to new shapes, less experimental and theoretical validation has been done for how well RUS works when boundary conditions (like clamping or supports) are applied.

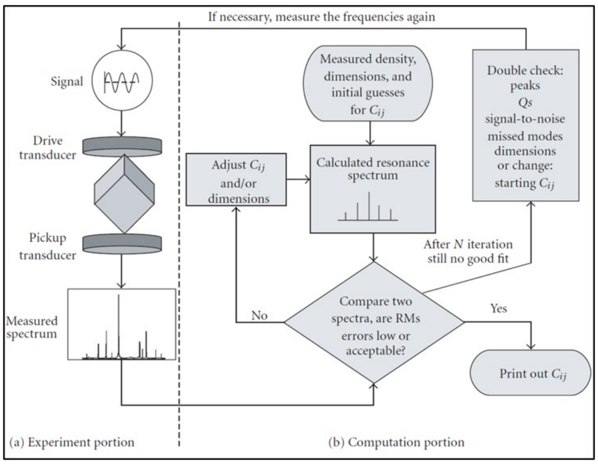

Fig. 1 The figure from [1] shows a traditional workflow output for a RUS experiment

Table 1 Experimental Factors for RUS Study

Conventional RUS	FEA with RUS
Swept Sine Input	Swept Sine Input
Free-Free Boundary	Prescribed Boundary
Frequency Spectra	Frequency Spectra
Simple Geometries	Complex Geometries
Single Point Excitation	Multi Point Excitation

This study aimed to validate RUS's ability to identify characteristics for metallic samples with boundary conditions to boost its reliability for advanced material applications. Comparing free and constrained vibration data from metallic samples allowed assessment of RUS accuracy and reliability when boundary conditions are introduced. Our goal was to evaluate the performance of RUS for determination of material properties under fixed boundary conditions. We specifically tested this through comparison of RUS experiments on an high purity aluminum rod under free-free and applied cantilever boundary conditions.

Background

This project aimed to expand RUS to accommodate non-idealized experimental boundary conditions. Validating performance for these boundary conditions would enhance RUS reliability for advanced material manufacturing applications and extend its capabilities to real-world manufacturing environments. This development could benefit on-machine inspection throughout

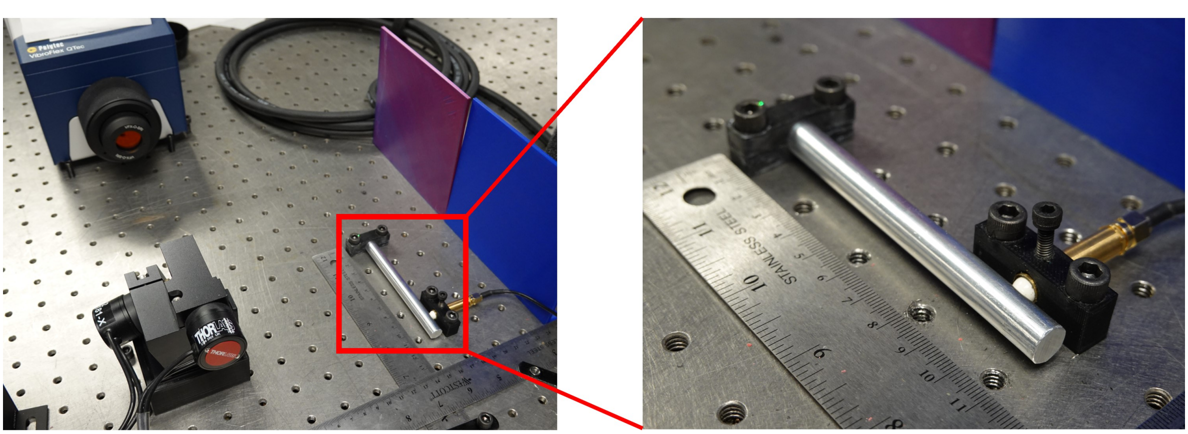

Fig. 2 Experimental apparatus for boundary conditioned RUS

the production process, significantly reducing handling risks and improving quality control. A key example of such non-ideal conditions is found in lathe operations, which our group explored in this study. The boundary condition in a lathe scenario is closely associated with a surface area prescribed boundary contact - to examine the lathe-inspired boundary condition, we devised an experimental setup that simulates these conditions, as shown in Figure 2. This setup allowed us to analyze how such boundary conditions affect RUS measurements and thus material property extraction, thereby bridging the gap between laboratory-based RUS and its practical application in manufacturing settings.

Our experimental setup featured a clamshell design with 3D printed PLA detachable top and bottom halves. This design prioritizes simplicity, utilizing just two protruding bolts for secure mounting. The streamlined configuration offered multiple benefits, including improved signal-to-noise ratio, enhanced laser scan results, and clearer mode shape visualization. A key feature of the setup is the 3D printed transducer stand, intentionally designed to be separate from the sample holder. This strategic separation minimizes the transmission of external vibrations to the clamp, thereby reducing unwanted noise and preventing the excitation of undesired mode shapes. Together, these design elements contribute to more accurate and reliable measurements in our RUS experiments.

Table 2 illustrates our mode shape extraction process. To obtain accurate mode shapes, we employed a Polytec 1D Qtec LDV connected to a Polytec VibroFlex Connect Front-End (max. frequency bandwidth of 24 MHz), coupled with a dual-axis galvanometer mirror system from Thorlabs to enable scanning. This technique allowed us to extract detailed 2D modal data, providing a comprehensive view of the material's vibrational behavior under various conditions. Table 3 shows a representative example of the difference between free-free and cantilever boundary for an experimental mode. The color distribution along the sample represents the displacement of the specimen. Red locations mean there is high displacement, and blue locations represent low displacement areas.

Table 2 Mode Shapes Extracted Using LDV

Mode Shape	Mode	Frequency (kHz)
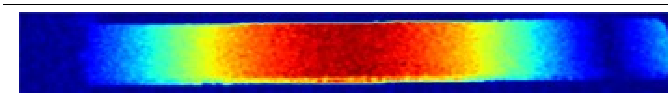	2	2.83
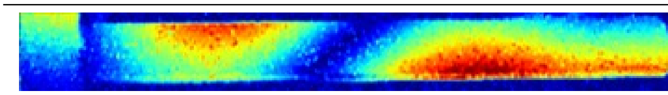	11	9.81
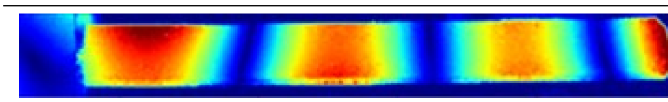	14	16.98
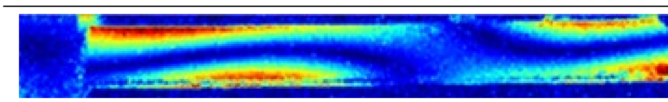	18	21.36
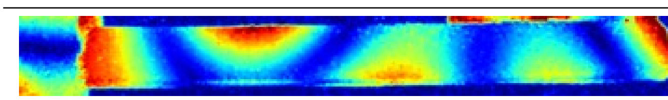	21	24.49

Table 3 Comparison between a free-free and cantilever mode shape

Free-Free	Cantilever
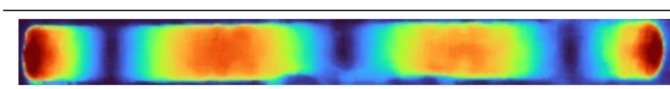	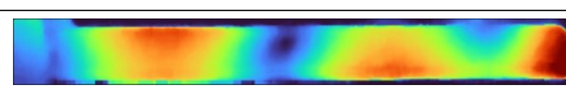

Experimental Methods

Figure 3 illustrates our project's experimental workflow. The process began with data extraction using the RUS holder under two conditions: free vibration and fixed boundaries. To collect the frequency spectrum from a specimen we placed our high purity aluminum bar between the two clamshell PLA holders and bolted it directly into the optical table. We tightened the bolts to 2 N-m of torque for each trial to ensure repeatability and full contact. After this the LDV was aimed at the aluminum specimen at the 8 cm point from the fixed end, that was determined from an optimization study, at which point the frequency excitation began. We used previously determined settings to collect data which was then exported to begin the mode experimental mode shape scans. The resonant peaks were identified and then utilized in the laser scan software to obtain the mode shapes of the specimen. After this the frequency and mode shape data were exported into python scripts for processing. This experimental data was qualitatively compared against the scanned mode shapes to validate our approach. We then assessed the accuracy of the extracted data relative to our theoretical model, evaluating RUS's capability to determine material properties under various boundary conditions.

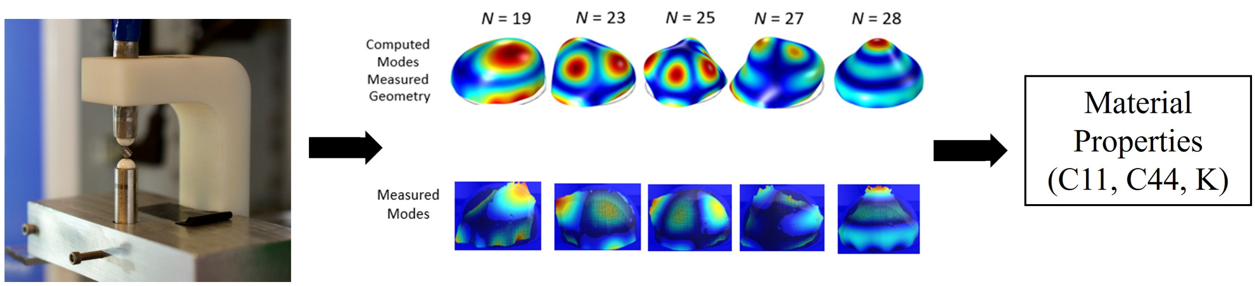

Fig. 3 Setup from LA-UR-23-22399 [2]. Mode shape images from [3]

Experimental Apparatus

Table 4 outlines the control group and variables for our experiment. To ensure the reliability and validity of our results, we carefully controlled key factors including material selection, specimen geometry, transducer and clamping locations, and clamping force. By maintaining consistency in these control variables, we aimed to isolate the effects of our independent variables on the resonant behavior of the specimens.

Table 4 Experimental Control Groups

Variable type	Factors
Independent	Boundary Conditions (fixed vs free) Specimen and Fixture Contact type (point vs surface) Fixture location (point, edge, corner)
Dependent	Resonance Frequencies (Hz) Mode Shapes Q factor/Damping Inversion Error
Control	Material Selection Geometry Transducer/Clamping location Clamping force

This experimental design allowed us to evaluate the sensitivity of the RUS technique to various boundary conditions and contact configurations, providing insights into its robustness and applicability in different scenarios. In our experimental apparatus there were a variety of devices that were utilized to perform RUS experimentation. In Table 5 you can see a list of the devices used as well as the role the device played in our experiments.

Evaluation of different experimental setups required experimental repeatability from run to run. This was partially accomplished through control over parameters and settings. Sample excitation was controlled via a consistent transducer drive amplitude of 5 Vpp to ensure that the high purity aluminum specimen was fully excited. The frequency range that we collected data over was from 100 Hz to 60 kHz. Starting at 100 Hz ensured that low frequency modes and shifted modes would

Table 5 Experimental Equipment and Setup

Equipment	**Function**
Piezoelectric transducers	Vibration input/excitation
Function Generator/Oscilloscope	Sweep through frequency range
Mounting apparatus / Frame	To position sample freely or constrained
Laser Doppler Vibrometer (LDV)	Contactless measurement of velocities
FEM software (Abaqus)	Simulate and invert modes
Calipers and Scale	Precise sample measurement
Environmentally Controlled Lab	Indirect control of temperature, humidity, and vibration isolation

be captured. The final frequency of 60 kHz was chosen after doing a sensitivity analysis which determined that modes after the 18th mode, which occurred at roughly 58 kHz, provided no new meaningful data. A frequency step of 2 Hz was selected to maintain the true center-to-center peak width for attenuation analysis. The ring-up time and acquisition time were set to 40 ms and 20 ms to ensure that full excitation was reached and captured. Given these settings, each run took approximately 40 minutes.

LDV parameters were optimized and then held constant during the experiments. The bandwidth was chosen to be 100 kHz, to ensure that we were fully capturing the full range of frequencies that were swept through during testing. Once the LDV was set, we maximized the instrument sensitivity by minimizing the velocity range. A range of 5 mm/s resulted in a sensitivity of, 2.5 mm/s/V. For our testing, we found that these settings provided sufficient sensitivity and produced reliable results.

There were five key criteria for choosing a metal sample for RUS experimentation. The first was elastic isotropy which was important for ease of analysis. The next criterion was homogeneity. While RUS can easily characterize alloys in a free-free regime we wanted to minimize the complexity of the specimen in a cantilevered regime. The next factor considered was a material that had high Q factors, which pointed us in the direction of metal specimens. The next two criterion are less restrictive as they can be easily characterized for each material. Having known specimen size and geometry ensure that models and RUS inversions are accurate. Based on this criterion, we chose a polycrystalline isotropic high purity aluminum sample for our RUS experiments due to its optimal properties. Its high purity minimizes internal defects, while its isotropic nature ensures uniform elastic properties (C11, C44) across all directions. The material's low natural damping and high Q factor result in sharp, easily identifiable frequency peaks. These characteristics collectively simplify analysis, improve measurement accuracy, and enhance the overall reliability of our RUS studies.

The 3D printing parameters utilized in our experiment were carefully selected to ensure the specimen fixtures were consistent and maximally rigid. The 100 percent infill density ensures that the fixture will be solid throughout, providing maximum stiffness and stability. At lower infill densities, the reduced stiffness allows the specimen to have increased motion which could reduce the quality of the frequency response. This is crucial for modal analysis as it minimizes any potential interference or unwanted vibrations from the fixture itself, allowing for more accurate measurements of the test subject's natural frequencies and mode shapes. Printing with a 100 percent infill also allows for the approximation of isotropic material properties. Although this assumption is not quite true as layer to layer interactions, internal voids, and other factors make the plastic anisotropic; these effects are minimized for small parts like our holders.

There are a variety of infill structures that can be used when printing with an FDM printer. The gyroid pattern provides isotropic strength properties, meaning it has similar strength in all directions. This is particularly advantageous for a modal analysis fixture, as it helps to distribute forces evenly and minimize any directional bias in the fixture's response. Additionally, the gyroid structure offers a good balance between strength and weight, which can be beneficial in reducing the overall mass of the fixture while maintaining its structural integrity.

The contact interfaces between the plastic parts and the metallic components of our apparatus needed to be as smooth as possible to ensure uniform contact. As can be seen in Figure 4 the 3D printed parts had contact areas printed in the Z direction to eliminate the need for supports at those locations. The print orientation in tandem with a chemical smoothing performed in acetone produced very smooth interfaces. The print orientation is also beneficial as it optimizes the strength of the fixture along its primary axis of loading. This orientation takes advantage of the layer-by-layer printing process, aligning the layers perpendicular to the main forces experienced during testing, which enhances the fixture's overall structural integrity.

We chose to use PLA for multiple reasons. The first is that the plastic is easy to print, has dimensional stability, and relatively high stiffness when compared to other plastics. We performed a plastic analysis study to see if ABS would be

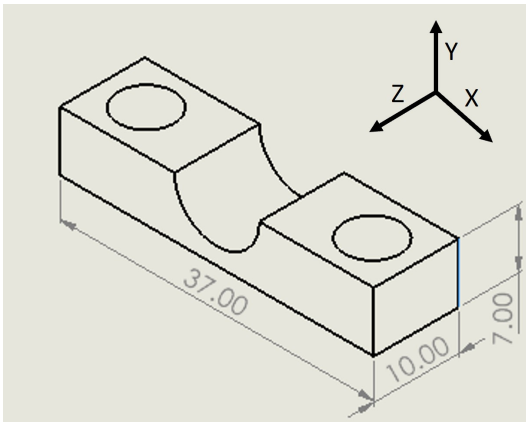

Fig. 4 Image of the print orientation of PLA components with units in mm

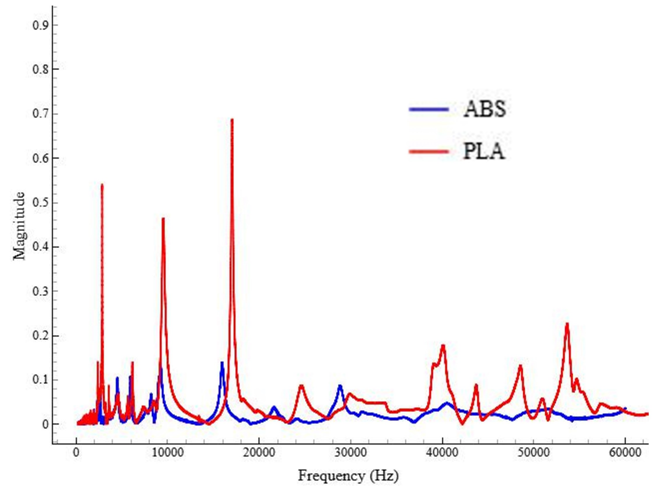

Fig. 5 Frequency response plot for the same frequency excitation sweep in the PLA and ABS holding fixtures

a more suitable material for our fixtures. ABS has a lower tensile strength than PLA but a higher flexural modulus and a larger elongation at break. We did this by testing six different aluminum samples in identical fixtures except for the plastic that it was made from. You can see in Figure 5 that the PLA holding fixture had a higher magnitude response which makes peak identification significantly easier. The ABS attenuated the signal response from all six specimens which increased the prevalence of noise in the response. There was a similar amount of peak shifting present in both holders due to stiffness and mass, which led us to the conclusion that PLA was the best material to use in our experimental apparatus.

After determining all the relevant parameters for the plastic and hardware, we moved on to finding the optimal location to have the laser beam on the specimen. This was done by placing the transducer 9 cm from the fixed end of the aluminum specimen. After this the LDV was aimed at a point 10 cm from the fixed end of the bar after which the specimen was excited. Following this, the laser was moved 2 cm down the bar closer to the fixed end, the measurement cycle was performed and this

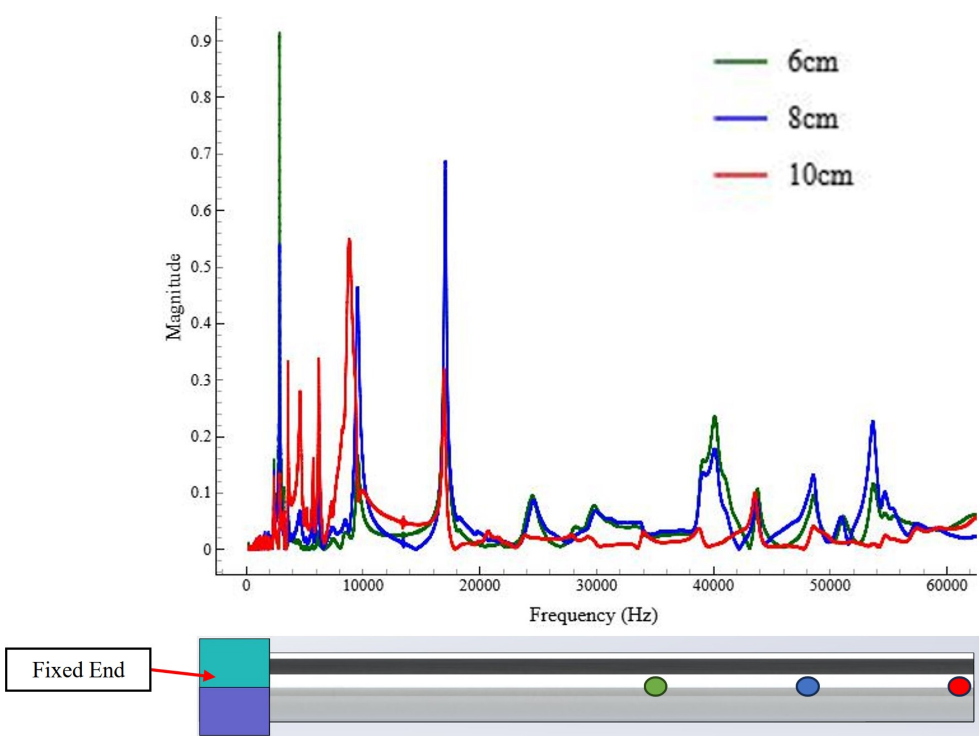

Fig. 6 Laser sweep study to determine the optimal laser location

process was repeated until the fixed end was reached. Figure 6 is a plot comparing the first three points along the specimen that were scanned. The largest difference that can be seen is in the amplitude of the magnitude for each response. The scan at the end of the bar had the lowest magnitude amplitude responses as it underwent the most motion and the LDV would have signal quality fluctuations that increased the level of noise recorded. The scan at 8 cm had the second highest signal to noise ratio with distinct peak amplitudes. As you moved past the 8 cm point, low frequency peaks had higher amplitudes. However, some mode loss occurred as some small amplitude modes were no longer visually present (e.g 14 kHz in the 6 cm scan). This led us to decide on a final position for the laser at the 8 cm point (0.5 cm repeatability) to maintain the highest signal strength.

Finite Element Model

To assess the accuracy of our experimental mode shape data, our group developed Finite Element models for both a freely vibrating aluminum sample and a sample with prescribed surface boundary conditions. This comparative approach allowed us to validate our experimental results against theoretical predictions. The Finite Element models were created using industry-standard software, Abaqus, using published material properties of aluminum and the specific dimensions of our samples [4, 5, 6]. We simulated various vibrational modes for both the free and constrained conditions, paying particular attention to the differences in mode shapes and resonance frequencies between the two configurations.

Initially we modeled our system with a simple fixed end boundary condition, however it was later determined that the effects of damping in our apparatus made this modeling method invalid. We then moved towards complex damping modeling but found that it was too difficult to directly quantify the damping in our system without doing computationally expensive non-linear modeling. We then modeled the cantilevered bar by developing a system of springs to replicate the motion of the bar when under the cantilever boundary condition. In Figure 7 you can see the full model of our 6 Degree of Freedom (DOF) spring ABAQUS model. In this model we make several key assumptions to create an intermediate linear representation of the system. We assume these springs behave linearly, neglecting potential nonlinear effects that may arise in real-world scenarios. This simplification allows for a more straightforward analysis while still capturing the essential dynamics of the system. As can be seen in purple, we utilize a Reference Point to define a single point that governs the motion of the entire rigid body, simplifying the analysis of the object's overall behavior. This point is internal to the volume of the bar and is radially connected to numerous nodes along the entirety of the clamped area. We used a kinematic coupling to ensure that the motion of the reference point was properly replicating the motion of the bar. We then modeled the stiffness of the holder by using a system of linear springs, representing each of the six degrees of freedom, which can be seen on the right. Three of these springs represent the translational degrees of freedom and the last three represent the rotational degrees of freedom. On the right we have another spring in the X direction that replicates the force that the transducer imparts during excitation of the specimen. This ensures that we capture the true dynamics of the system and replicate reality.

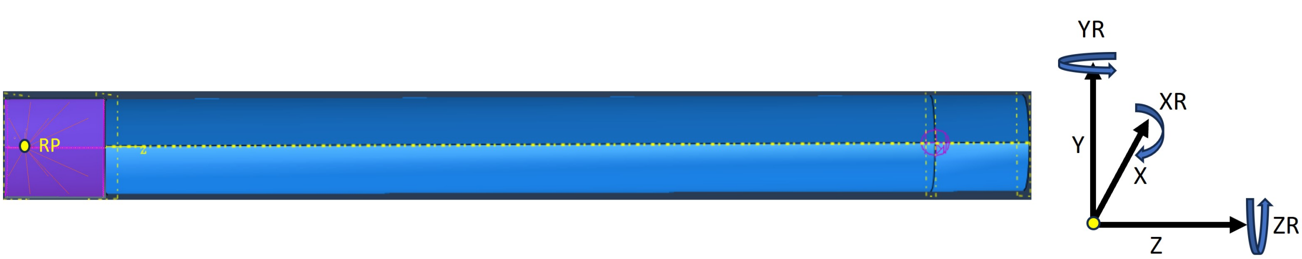

Fig. 7 This figure shows the full Abaqus model for the cantilevered specimen with the kinematic coupling shown in purple and the 6 translation and rotation springs to the right

By focusing on linear behavior, we created an intermediate model between free and prescribed boundary conditions that balances computational efficiency with a reasonable approximation of the system's response. This overall provides valuable insights into the specimen's vibrational characteristics without the added complexity of nonlinear analysis. A large part of this characterization was handled during the optimization of the spring stiffnesses. Since our model is somewhere between a free-free and fixed boundary condition the stiffness of each of the spring had to be manually tuned to match the experimental data.

The stiffness optimization was done manually through resonant frequency peak comparisons. As can be seen in Table 6 we tuned each spring stiffness for the first 15 modes to minimize the average percent error for the modes as well as maintaining a relatively distributed level of error across all the modes. Each spring was initially set to a value of 1e9 N/mm

Table 6 Spring Stiffness Optimization Table

Mode	Simulated Frequency (Hz)	Experimental Frequency (Hz)	Percent Difference (%)
1	3228	4266	27.7
2	3277	5936	57.7
3	7097	7338	3.4
4	8121	8222	1.2
5	9276	9152	1.4
6	10791	11346	5.0
7	12395	13398	7.8
8	17852	16536	7.7
9	18297	18272	0.1
10	21254	21962	3.3
11	26090	24520	6.2
12	28282	28018	0.9
13	34587	29494	15.9
14	35292	32746	7.5
15	37105	33172	11.2

which replicated a true fixed boundary condition. We started by characterizing each mode's sensitivity to each of the springs to see if the behavior was linear. Each mode had an initial linear response before converging to a constant frequency per mode. Each stiffness had a differing effect on the frequency response of the system. The stiffnesses with the highest effects were the X-translation DOF and the transducer spring. The next springs that had a significant effect on the response were the Y and Z translation degrees of freedom and the X and Z rotational degrees of freedom. The spring that had the smallest impact was the Y rotational DOF. In Table 7 you can see the final spring stiffness values that were utilized in the model.

Table 7 Final Spring Stiffness Values

X Stiffness (N/mm)	Y Stiffness (N/mm)	Z Stiffness (N/mm)	X Rotational Stiffness (N/mm)	Y Rotational Stiffness (N/mm)	Z Rotational Stiffness (N/mm)	Transducer Stiffness (N/mm)
1 E5	25 E5	75 E5	10 E5	250 E5	80 E5	5 E5

After this optimization was completed, we visually compared mode shapes for both the optimized modes, and modes outside the optimization selection. We found that we had qualitative agreement between the models which led us to do a final average percent difference calculation. The average value of 10.5% which was determined to be an adequate value as the model itself was accurately predicting the dynamic response of the system. Ignoring the first two modes as outliers, which we believe were unreliably captured by our experimental setup, reduced the average percent difference to 5.5%.

Results and Analysis

We conducted several experiments using free-free boundary conditions to verify both the material properties of our high purity aluminum and our capability to perform a RUS inversion. We extracted a range of values for the elastic tensor components C11 and C44 using the first 18 modes and used them to calculate the corresponding range for the Bulk Modulus of our material using Equation 1.

$$K = C_{11} - \frac{4}{3}C_{44} \tag{1}$$

Figure 8 displays a frequency spectrum from our experimental free-free setup. Additionally, the results calculated from the free-free experiments were compared to literature to confirm their accuracy and are shown in Table 8.

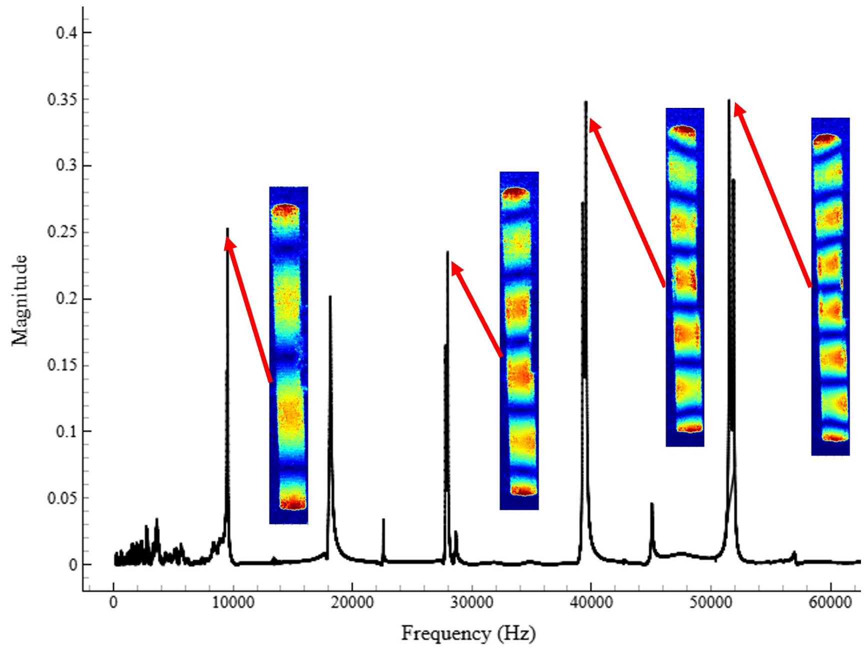

Fig. 8 Free-Free Frequency Spectrum

Table 8 Elastic Moduli for high purity aluminum. Literature values taken from sources -[4, 5, 6]

	C11 (GPa)	**C44 (GPa)**	**Bulk Modulus (GPa)**
Experimental	98.7 ± 5.3	25.9 ± 0.5	63.95 ± 4.45
Literature	91.9 – 104	23.3 – 26.3	60.8 – 68.9

The significant overlap between the experimental and literature values shown in Table 8 indicate that we were successful in measuring our material properties and ability to conduct a RUS inversion using a free-free boundary condition. We then proceeded to test our cantilever setup with prescribed boundary conditions.

We performed several tests in our cantilever setup after ensuring repeatability, and discovered a discrepancy in the modal data. An extra mode was occurring in the frequency spectrum at low frequencies caused by the transducer which was identified through analyzing the magnitude and phase plots of our mode shapes. To confirm this finding, we performed several tests using different aluminum samples to determine whether the resonance peak consistently reappeared in our frequency spectra. The data shown in Figure 9 confirms a recurring mode around 2.75kHz that was measured consistently across different aluminum sample tests. Table 9 provides supporting evidence, showing a false mode in the magnitude mode shape plot that doesn't appear in the phase plot of the aluminum sample. We confirmed that the mode originated from the transducer by taking mode shape scans on the transducer stand, specimen holder, and transducer. Because the transducer mode was not a characteristic of the high purity aluminum specimen, it was ignored in our analysis.

After all anomalies were identified, we performed a high fidelity scan of the cantilever setup to analyze for an inversion. Since established analytical methods to perform a RUS inversion assume free-free boundary conditions, we were unable to perform a traditional inversion to extract our material properties. Instead, we used a previously developed python script that used a finite element model as the forward solution with a genetic algorithm for the inversion. An initial finite element model was created in COMSOL using a fixed cantilever boundary condition. However, when attempting to match the experimental and simulated modes, resonance frequencies did not appear in the same regions and mode shapes did not correspond with each other. Additionally, we noticed immediate effects from the boundary conditions in the frequency spectrum of our cantilever experiment. RUS detects damping by measuring the full resonance response, including both the frequency and the

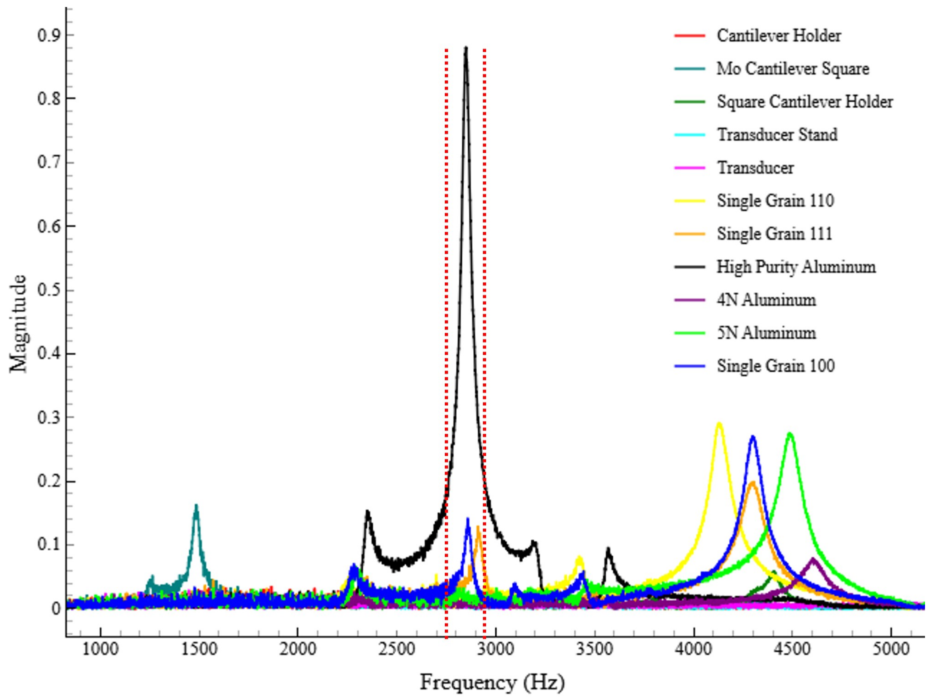

Fig. 9 Spectrum of Various Aluminum Samples

Table 9 Magnitude and Phase for Transducer Mode

Magnitude	Phase	Component
		
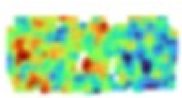	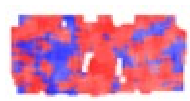	
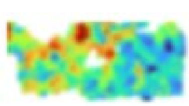	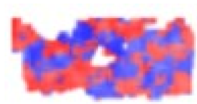	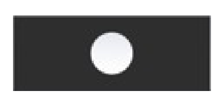
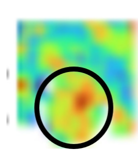	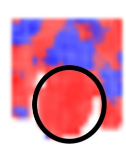	

width of resonance peaks. Damping affects the accuracy of RUS measurements in several ways: it broadens peaks, making precise center frequency determination more difficult; it reduces signal amplitude, potentially lowering the signal-to-noise ratio; and in highly damped systems, resonance peaks may overlap, challenging the isolation of individual modes.

Figure 10 shows a comparison between the free-free and cantilever frequency spectrum where the damping effects are present. In the cantilever frequency response, the peaks were heavily attenuated by the holding fixture resulting in reduced signals. The peaks were also shifted left and right from the presence of added mass and stiffness. The effects of damping on our system were characterized as non-linear preventing us from performing a RUS inversion. As a result, we shifted our focus towards analyzing these non-linear effects through both quantitative measurements and qualitative comparisons. Q factors and frequency shifts were used for quantification, while mode shapes were used for qualitative analysis.

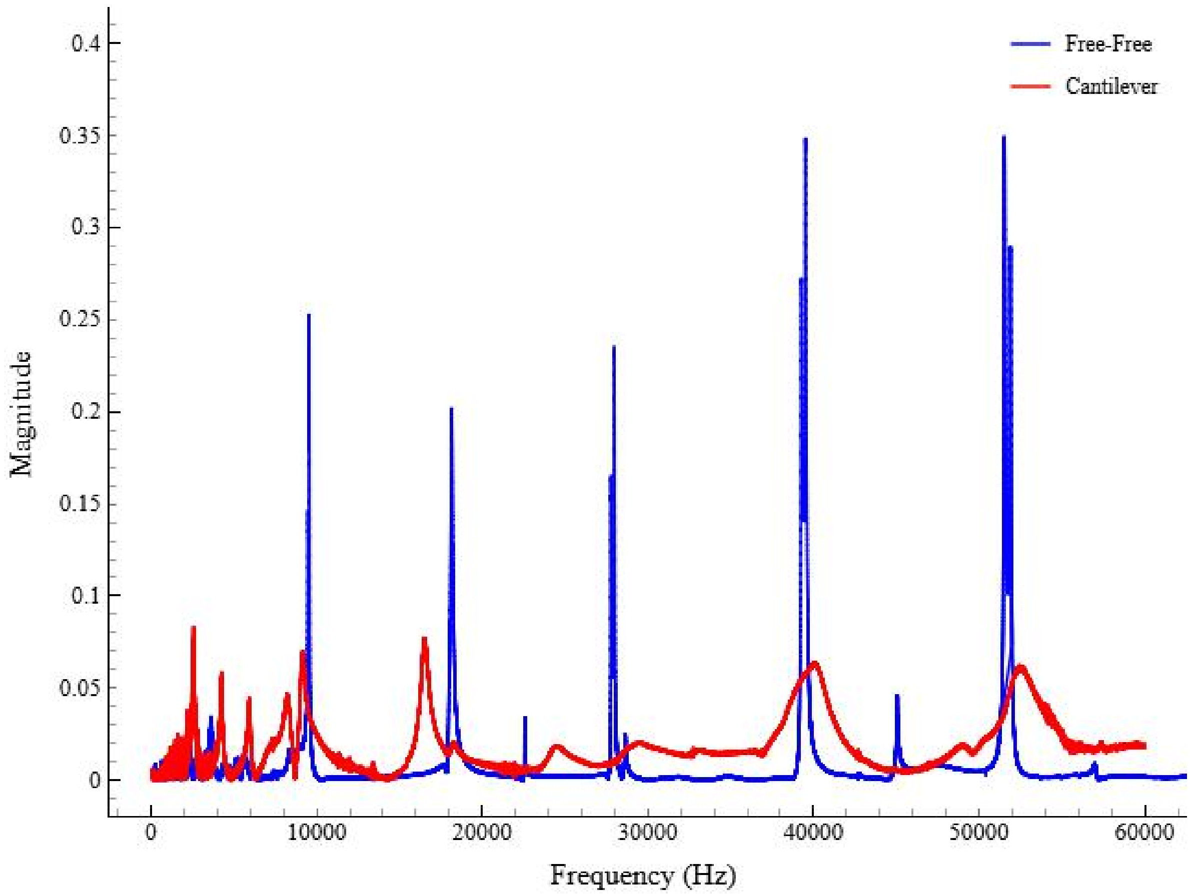

Fig. 10 Free-Free vs Cantilever Frequency Spectrum

We utilized our tuned finite element model to see if our model was closer to a free-free or fixed regime. As can be seen in Table 10 our specimen's response is closer to the response for a fixed specimen but not identical. The mode has the same shape but the actual magnitudes between the cantilever and fixed response are not the same. The most significant difference occurs at the clamping point where you can see in the cantilever response there is motion in the specimen that is not present in the fixed response. This motion is due to the specimen being stiffer than the holding fixture which allows for motion in the 6 degrees of freedom that we analyzed.

Q factors allow us to compare system damping where a higher Q factor indicates lower damping and good signal-to-noise ratio. High Q factors produce sharper resonance peaks and narrower bandwidths. We calculated our experimental Q factors using Equation 2 where f_o represents the resonance frequency and BW is the bandwidth of the peak, measured (in Hz) as the full width at half maximum (FWHM). The Q factors were then related to damping through Equation 2 where ζ represents the damping ratio. There is also an intrinsic impreciseness of frequency determination in dissipative systems, on the order of $1/Q^2$, stemming from the ambiguity in defining the resonance frequency due to damping [7].

$$\mathrm{Q} = \frac{f_o}{BW} = \frac{1}{2\zeta} \tag{2}$$

The Q factor for the free-free apparatus is 343.1 as compared to the Q factor for the cantilever apparatus of 18.76. We found the average Q decreased by 94.5% when compared with the free-free conditions, indicating significant damping effects in our system when applying prescribed boundary conditions. Additionally, there was a trend in the resonance frequency shift between the systems. While RUS can detect and measure damping, including friction damping, the presence of damping distinctly affects the accuracy of the measurements. The accuracy is primarily limited by the signal-to-noise ratio and the quality factor of the resonances, with an ultimate limit set by the intrinsic ambiguity in defining resonance frequencies in damped systems. The ability of RUS to achieve high signal-to-noise ratios can often offset some of the accuracy challenges posed by damping.

Table 10 Finite element simulation for Mode 6 in multiple loading scenarios

Free-Free	Cantilever	Fixed
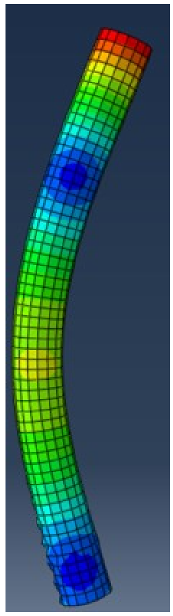	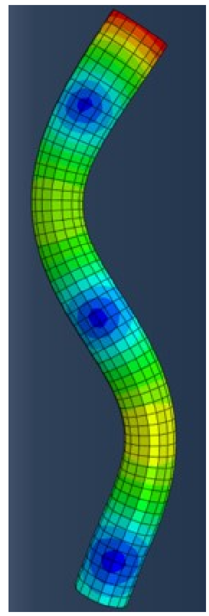	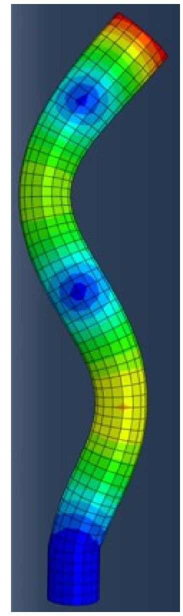

Conclusion

Our team successfully extracted and verified material properties for the high purity aluminum rod under free vibrating conditions using RUS. However, RUS's limitations in handling transient terms and complex boundary conditions necessitate further development to expand its applicability. Our team was able to extract information of the effects of boundary conditions, such as damping produced from the contact interface and frequency shifts. Future recommendations that can help advance this research involves changes to the experimental setup, data acquisition process, and inversion algorithm. Due to the lack of stiffness in our fixture, we were unable to fully qualify our boundary condition as fully cantilever. This leads us to recommending the use of a stiffer fixture such as a lathe or pipe vise to ensure that the specimen is fully fixed removing variability in the type of boundary condition being applied. Another limitation in our research was the ability to only measure out of place motion with our laser Vibrometer. Using other techniques such as Digital Image Correlation (DIC) would allow us to capture 3D displacement to identify any modes we might be missing compared to our signal point measurement technique. Additionally using triaxial accelerometer small enough for minimal mass loading could be another option to consider. As for inversion algorithms, we were unable to perform an inversion using established analytical methods as they are tailored for experiments that have free-free assumptions. Switching to a genetic algorithm which is a Stochastic evolutionary based algorithm, could help to converge to a global optimum rather than getting trapped in local minima. The genetic algorithm approach is particularly advantageous for our fixed-end cantilever configuration where the boundary conditions introduce additional complexity not accounted for in traditional analytical inversion techniques. Although our method was unsuccessful, we believe by pursuing these avenues, a RUS inversion can be successfully performed using boundary conditions.

Acknowledgments This research was funded by Los Alamos National Laboratory (LANL) through the Engineering Institute's Los Alamos Dynamics Summer School. The Engineering Institute is a research and education collaboration between LANL and the University of California San Diego's Jacobs School of Engineering. This collaboration seeks to promote multidisciplinary engineering research that develops and integrates advanced predictive modeling, novel sensing systems, and new developments in information technology to address LANL mission-relevant problems.

References

1. Li, G. and Gladden, J. “High temperature resonant ultrasound spectroscopy: a review”. *International Journal of Spectroscopy*, 2010(1):206362 (2010)ifnextchar.gobble.
2. Hayne Mathew Lindsay, e.a. “Error in rus measurements due to geometric uncertainties” (2023)ifnextchar.gobble.
3. Beardslee, L.B., Remillieux, M.C., and Ulrich, T. “Determining material properties of components with complex shapes using resonant ultrasound spectroscopy”. *Applied Acoustics*, 178:108014 (2021)ifnextchar.gobble.
4. Geimer Paul R, e.a. “Finite-element-based resonant ultrasound spectroscopy for measurement of multi-material samples”. *The Journal of the Acoustical Society of America*, 151(6):3633–3640 (2022)ifnextchar.gobble.
5. Kaufman, J.G. “Properties of pure aluminum” (2018)ifnextchar.gobble.
6. Hunsicker, H., Mondolfo, L., Tomblin, P., Carapella Jr, S., Hayduk, D., Carapella Jr, S., Hayduk, D., Westbrook, J., Marder, J., Stonehouse, A., et al. “Properties of pure metals”. In *Properties and Selection: Nonferrous Alloys and Special-Purpose Materials*, pages 1099–1201. ASM International (1990)ifnextchar.gobble.
7. Balakirev, F.F., Ennaceur, S.M., Migliori, R.J., Maiorov, B., and Migliori, A. “Resonant ultrasound spectroscopy: The essential toolbox”. *Review of Scientific Instruments*, 90(12) (2019)ifnextchar.gobble.

Appendix: Mesh Convergence and Q Factor Calculation

Table 11 Mesh Convergence Study: Relative Error in Natural Frequencies (Free-Free Vibration)

Number of Elements	Mode	Relative Error (%)			
		Mode 1	Mode 3	Mode 5	Mode 8
1819	1	0.014	0.028	0.036	0.000
2872	3	0.006	0.015	0.021	0.000
8924	5	0.000	0.002	0.000	0.000
29351	8	0.000	0.000	0.000	0.000

As shown in Table 11, the relative error decreases as the number of elements increases for free-free boundary condition vibration. The maximum relative error in natural frequencies compared to the finest mesh is 0.036%. This very small error indicates that even a coarse mesh is acceptable for this free-free vibration analysis.

Table 12 Mesh Convergence Study: Relative Error in Natural Frequencies (Cantilever Vibration)

Number of Elements	Mode	Relative Error (%)			
		Mode 3	Mode 7	Mode 10	Mode 14
7338	3	0.4635	0.4492	0.1744	0.4290
13398	7	0.2986	0.2898	0.0998	0.2776
21962	10	0.1472	0.1393	0.0404	0.1262
32746	14	0.0000	0.0000	0.0000	0.0000

As shown in Table 12, the relative error in natural frequencies decreases consistently as the number of elements increases for the cantilever boundary condition vibration analysis. The finest mesh (27,915 elements) is used as the reference for error calculation. The maximum relative error observed is approximately 0.4635% for Mode 1 with the coarsest mesh (2,133 elements), while the minimum error is 0.0404% for Mode 5 with 9,157 elements. This trend demonstrates clear mesh convergence, with even the coarsest mesh providing reasonably accurate results. The rapid decrease in error with increasing element count suggests that a moderately fine mesh offers a good balance between accuracy and computational efficiency for this cantilever vibration analysis.

$$\mathrm{Q} = \frac{Resonant Frequency}{Bandwidth} = \frac{27000Hz}{27256Hz - 26743Hz} = 52.63 \tag{3}$$